Enhanced Aerosol Mass in the Tropical Tropopause Layer Linked to Ozone Abundance

Shang Liu[1,*], Troy D. Thornberry[2], Pengfei Yu[3], Sarah Woods[4], Karen H. Rosenlof[2], and Ru-Shan Gao[2,*]

[1]Department of Civil and Environmental Engineering, Northeastern University, Boston, MA 02115, USA
[2]NOAA Chemical Sciences Laboratory, Boulder, CO, USA
[3]Institute for Environmental and Climate Research, Jinan University, Guangzhou, China
[4]Earth Observing Laboratory, National Center for Atmospheric Research (NCAR), Boulder, CO

*Correspondence author: shang.liu@northeastern.edu, rushan.gao@noaa.gov

Key Points:
- Aircraft measurements reveal persistent enhancement of aerosol mass in the TTL.
- The TTL aerosol enhancement tightly correlates with ozone. An empirical parameterization of TTL aerosol as a function of ozone is derived.
- Modeling suggests that TTL aerosol particles are mainly composed of organics and sulfate.

Abstract

Aerosol particles play a critical role in the tropical tropopause layer (TTL) through cloud formation and heterogeneous chemistry, influencing the radiative and chemical balance of the stratosphere. However, aerosol measurements in the TTL are sparse, resulting in poor knowledge of aerosol abundance and distribution in this important region. Here, we present in situ aircraft measurements over the western tropical Pacific, revealing a persistent and altitude-dependent enhancement of aerosol mass in the TTL compared to the convectively influenced troposphere below. Notably, our data demonstrate a striking positive correlation between aerosol mass and ozone. Model simulations suggest that organic materials constitute a substantial fraction of the total aerosol mass within the TTL. We further derived an empirical parameterization of TTL aerosol mass as a function of ozone. Given the relative ease of ozone measurements and modeling, the parameterization provides a promising framework for estimating TTL aerosol abundance and its effects on climate.

Plain Language Summary

We investigated tiny particles called aerosols in a specific atmospheric layer called the tropical tropopause layer (TTL). These particles are crucial because they affect cloud formation and chemical processes in the atmosphere, influencing how energy is distributed. Unfortunately, there hasn't been much research on aerosols in the TTL, leading to gaps in our understanding of their abundance and distribution in this important region. To fill this knowledge gap, we conducted measurements using aircraft over the western tropical Pacific. Our findings revealed that aerosol

mass in the TTL is consistently higher compared to the lower troposphere, which is influenced by upward air movement. What's interesting is that we observed a clear connection between the amount of aerosol and ozone. Our model simulations indicated that a significant portion of the aerosol mass in the TTL is made up of organic materials. To make it easier to estimate aerosol levels and their impact on climate, we developed a way to predict TTL aerosol mass based on ozone measurements. Since ozone is relatively straightforward to measure and model, our method could provide a useful framework for understanding aerosol abundance in the TTL and its effects on the climate.

1 Introduction

As the main pathway for the transport of tropospheric air into the stratosphere, the TTL largely determines the entry values for the materials entering the stratosphere (Fueglistaler et al., 2009). The properties of the TTL air and the processes occurring in the TTL thus affect the global stratosphere and climate (Randel and Jensen, 2013; SPARC 2006).

Aerosol particles in the TTL affect the stratospheric water vapor budget through TTL dehydration processes by serving as nuclei for the formation of cirrus clouds (Penner et al., 2009). TTL circus clouds have substantial impacts on the earth's radiative balance (Hong et al., 2016). By providing condensed surface areas, TTL aerosol can also facilitate condensation of low vapor pressure gases such as sulfuric acid (Brock et al., 1995) and promote heterogeneous chemistry that depletes ozone once they are transported to the stratosphere (Tolbert et al., 1988). Despite the importance, the abundance and properties of the TTL aerosol remain poorly characterized. Field observations have suggested that new particle formation events frequently occur in the TTL, in particular the lower TTL just below the tropopause (Brock et al., 1995; Weigel et al., 2011, 2021). The composition of the TTL aerosol is influenced by tropical dynamics (e.g., transport) and regional continental air sources (Froyd et al., 2009). Recent advancements in SO_2 measurement in the TTL suggests little contribution of SO_2 to stratospheric aerosols, revealing a significant gap in the stratospheric aerosol budget (Rollins et al., 2017). The complex dynamic and chemical processes in the TTL make it difficult to elucidate the formation mechanisms of the TTL aerosol. In-situ measurements of TTL aerosol are limited, hindering our understanding on the climate impacts of the TTL and stratospheric aerosols.

For this study, we carried out aircraft measurements of aerosols over the western Pacific warm pool during the Pacific Oxidants, Sulfur, Ice, Dehydration, and cONvection (POSIDON) campaign in October 2016. The western Pacific warm pool plays a leading role for transport of air into the TTL (Fueglistaler et al., 2005). Our measurements were carried out during nine flights aboard a NASA WB-57F high-altitude aircraft stationed in Guam. Throughout these flights, we extensively characterized TTL aerosols and trace gases (flight tracks are shown in Fig. 1). To complement the measurements, we employed modeling techniques to obtain insights into the chemical composition of the aerosols. The combined approach of aerosol measurements, tracer analysis, and modeling offers insight into aerosol abundance and formation mechanisms within the TTL.

2

2 Methods

2.1 Measurements

The POSIDON campaign, took place during October 2016, aimed at improving our understanding of the physical and chemical processes occurring in the TTL. A total of nine flights were carried out on board the NASA WB-57 high altitude aircraft from Guam (13.5° N, 144.8° E). These flights covered the region from 0 to 15°N and from 130 to 160° E (Fig. 1a), with vertical coverage spanning 0 to19 km (Fig. 1b). Each flight path consisted of several upward and downward segments between 14 and 18 kilometers in altitude, providing extensive sampling of the TTL. The measurement region lies over the tropical warm pool, where high sea surface temperatures lead to widespread deep atmospheric convection (Yan et al., 1992).
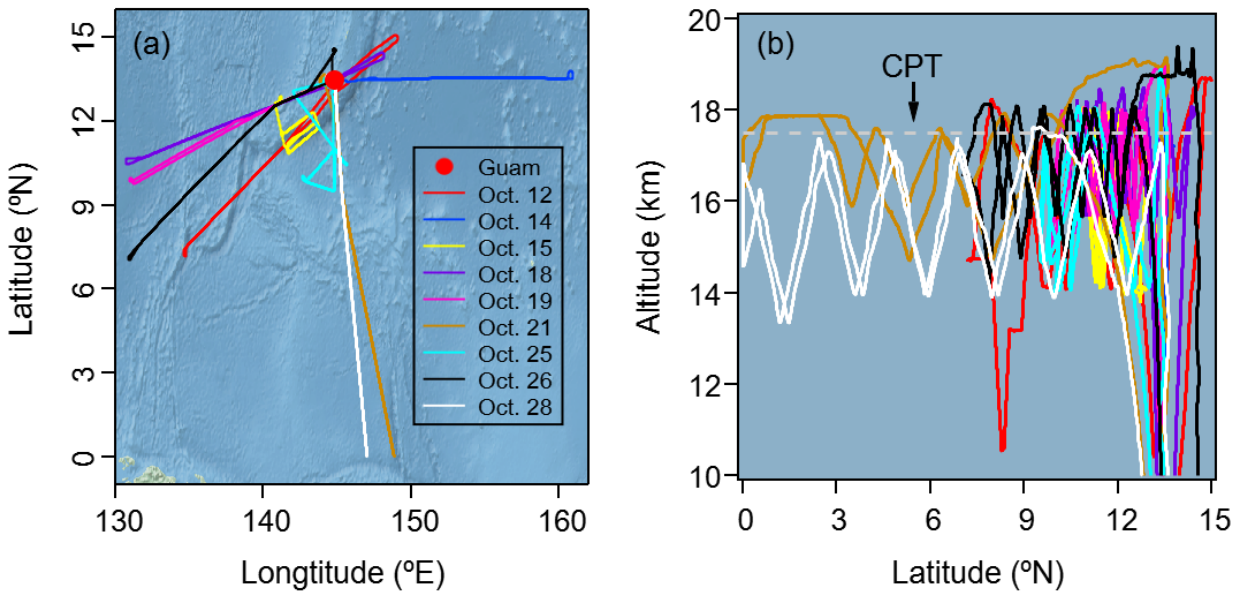

Figure 1. Flight tracks during the POSIDON campaign.

The aerosol particles were sampled through a near-isokinetic inlet that reduces the ambient sample speed from the aircraft speed of ~90–200 m s^{-1} to ~3 m s^{-1} while maintaining ambient aerosol mixing ratios (Jonsson et al., 1995). This inlet has been employed in various aircraft campaigns for aerosol sampling (e.g. Schwarz et al., 2006). Aerosol number size distribution was measured in situ by a custom-built optical particle counter, the portable optical particle spectrometer (POPS), which was mounted in the fuselage bay of the aircraft. The POPS uses a 405 nm laser to count and size individual aerosol particles with diameters from 140 to 3000 nm (Gao et al., 2016). The scientific application of the POPS has been demonstrated by recent field campaigns (Cui et al., 2018; Liu et al., 2021; Yu et al., 2017). In the POPS instrument, each particle passing across the laser beam produces a pulse by scattering the laser light. The particle number is determined by the number of the pulses. The particle size is calculated from the intensity of the pulse, which was calibrated using a series of differential mobility analyzer (DMA) size-selected dioctyl sebacate (DOS) particles prior to the campaign. The aerosol mass was calculated from the aerosol number and size assuming that the particles are spherical and have a constant density of 1.6 g cm^{-3}. The

mass mixing ratio (MMR) of aerosols was determined as the ratio of aerosol mass to the density of ambient air, which was calculated from the measured air pressure and temperature. A lognormal fit to the measured mass size distribution derived from the POPS measurements in the TTL (Fig. S1) suggests that the POPS measurements captured approximately 50% of the total aerosol mass. Laboratory tests suggest that the POPS instrument used during POSIDON can provide reliable measurements under pressures as low as 70 hPa, which corresponds to an altitude of 18.9 km in this study. Therefore the POPS data acquired above 18.9 km are not used in the analysis.

The size distribution of particles with diameter larger than 3 µm was measured with a fast cloud droplet probe (FCDP). The FCDP detects particle forward scattering to determine the number and size of particles (Lance et al., 2010; McFarquhar et al., 2007). We assume that all particles greater than 3 µm are ice crystals as the number of large aerosol particles in the upper troposphere is negligible (Jensen et al., 2013). We found that ice crystals could likely abrade the inlet materials, resulting in artifacts in POPS-measured aerosol size distribution. Such interference has been observed in previous aircraft measurements (Murphy et al., 2004). For this reason, we excluded the POPS data when ice crystals were present from the analysis.

Additional real-time measurements included: (i) ozone mixing ratio obtained using a custom UV spectrophotometer designed for high altitude airborne deployment with high accuracy and precision (Gao et al., 2012), (ii) water vapor mixing ratio measured by a two-channel tunable diode laser-based hygrometer, which is capable of accurately measuring low-concentration (below 1 ppm) water vapor in the upper troposphere and lower stratosphere (Thornberry et al., 2015), and (iii) ambient air pressure and temperature measured by the Meteorological Measurement System (MMS; Chan et al., 1989; Scott et al., 1990), which also records aircraft position with 1-second time resolution.

2.2 Modeling
We employed the Community Aerosol and Radiation Model for Atmospheres (CARMA), an advanced sectional aerosol model (Toon et al., 1988; Yu et al., 2015). CARMA is coupled with the Community Earth System Model (CESM), allowing for comprehensive analysis of aerosols. The model operates at a spatial resolution of $1.9° \times 2.5°$ and employs a time step of 30 minutes. The model incorporates 35 vertical pressure levels, spanning from the Earth's surface up to 200 hPa, and an additional 21 vertical pressure levels from 200 hPa to 2 hPa. Simulations are nudged to meteorology from Modern-Era Retrospective analysis for Research and Applications, Version 2 (MERRA-2; Gelaro et al., 2017).

CARMA tracks two groups of aerosols, with each group containing 20 size bins. The first group consists of pure sulfate particles with aerosol diameter ranging from 0.4 nm to 2.6 µm. These particles form through nucleation and condensation of water and sulfuric acid vapor (Zhao and Turco, 1995). The second group comprises internally mixed aerosols with the diameters varying from 100 nm to 17 µm. These mixed aerosols consist of particles that contain organic compounds, black carbon (BC), sea salt, dust, and condensed sulfate.

4

159 In addition, we employed a straightforward, observationally constrained chemical model to
160 characterize the vertical distribution of O_3 within the TTL. This model is a one-dimensional
161 column model that allows updrafts and vertical mixing but assumes no horizontal mixing. The O_3
162 formation process is represented using the Chapman mechanism, and O_3 profiles were calculated
163 for the altitude range of 14.5–18.9 km. A detailed description of the model is provided in the
164 Supporting Information.
165
166 **3 Results and discussion**
167
168 **3.1 Determination of TTL**
169 We adopt the upper boundary of the TTL to be at 19 km, following SPARC (2006). This altitude
170 is 2.5 km higher than the cold point tropopause (CPT) as shown in Fig. S2. The CPT corresponds
171 to an altitude of 17.5 km and air temperature of approximately 190 K. These values are in line with
172 previous measurements of TTL (Fueglistaler et al., 2009; Gettelman et al., 2004).
173
174 The lower boundary of the TTL is determined by examining the vertical profile of potential
175 temperature (θ; Fig. S3). The curvature of the altitude-θ profile changes at 14.5 km, which is
176 mathematically characterized as the lapse rate minimum (LRM) of θ. This change reflects the
177 transition of stability regimes, i.e., deep convection dominates air stability below the LRM and
178 radiation starts to influence air temperature above the LRM. Accordingly, we identify the LRM
179 level at 14.5 km (355 K, 140 hPa) as the base of the TTL (Gettelman and Forster, 2002), which is
180 consistent with previous studies (Fueglistaler et al., 2009; Sunilkumar et al., 2017). As a result, the
181 TTL spans from 14.5 km to 20 km, and the majority of our measurements were conducted within
182 the TTL (Fig. 1).
183
184 **3.2 Vertical profile of aerosols and ozone**
185 The vertical profile of aerosol mass from the surface to the top of the TTL can be segmented in
186 three layers with distinct characteristics (Fig. 2a). Layer I spans from the surface to 5 km altitude
187 and represents the lower troposphere, in which the MMR of aerosols decreased logarithmically
188 with altitude from 2 µg kg^{-1} to 0.08 µg kg^{-1} likely because of the influence of surface emissions
189 from Guam. Layer II ranges from 5 km to 14.5 km altitude. In this layer, the aerosol MMR
190 remained at approximately 0.08 µg kg^{-1} with small variability. Such low-concentration aerosol
191 layers immediately below the convection outflow have been observed previously over the
192 Northern Indian Ocean (de Reus et al., 2001) and the rain forests in South America (Andreae et
193 al., 2018; Krejci et al., 2003). The observation indicates that deep convection serves as an effective
194 sink for aerosol particles (Yu et al., 2019). Layer III lies in the TTL, extending from 14.5 km to
195 18.9 km, with the upper boundary 1.4 km higher than the CPT. In this layer the aerosol MMR
196 increased rapidly from 0.08 µg kg^{-1} at 14.5 km to 1.5 µg kg^{-1} at 18.9 km. Our observations show
197 a sustained increase of aerosol MMR from the upper troposphere to lower stratosphere across the
198 tropopause, rather than abrupt transitions. This suggests that the CPT has no unique role for the
199 transport of aerosols. Accounting for the mass of <140 nm particles that were not measured by the
200 POPS instrument, the aerosol MMR at 18.9 km would be approximately 3 µg kg^{-1}. This
201 concentration is close to the measurement during the POLARIS mission in 1997 (Mclinden et al.,

5

202   1999), in which an aerosol MMR of approximately 3.5 µg kg⁻¹ was observed for aerosols with size
203   range of 0.07–1 µm at 18.9 km in eastern Pacific (17.5° N, 159.3° W).
204
205   The ozone concentration remained below 35 ppb in layers I and II and began to increase at 14.5
206   km (Fig. 2b). This observation is consistent with previous ozonesonde measurements in the
207   tropical Pacific (Folkins et al., 1999; Folkins and Martin, 2005). The concurrence of ozone
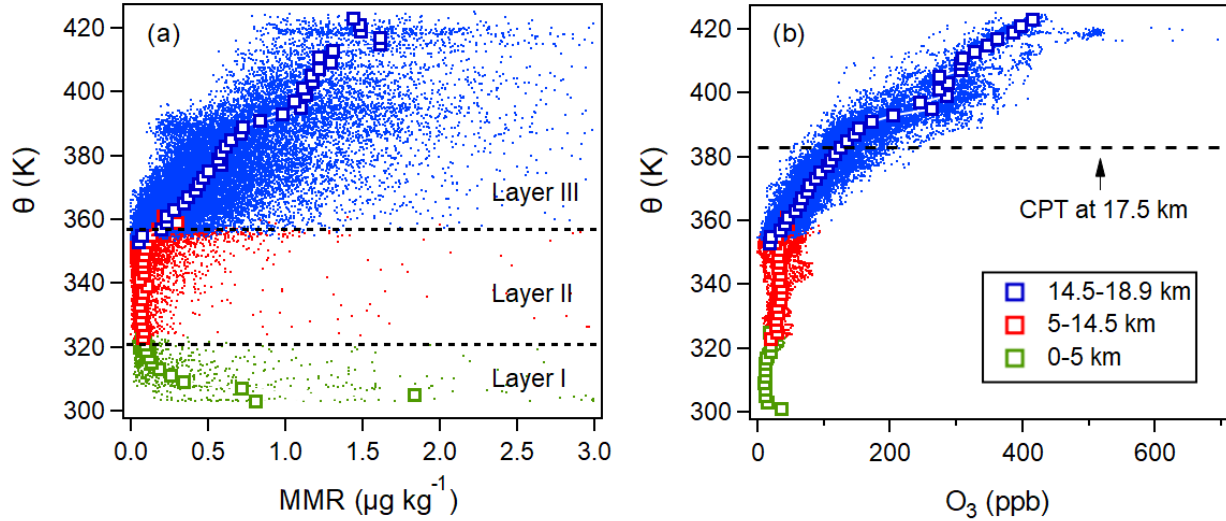208   minimum and LRM is in line with the analysis by Gettelman and Forster (2002) and Folkins et al.
209   (2002).
210

211
212   **Figure 2**. Potential temperature (θ) versus **(a)** O_3 and **(b)** MMR for data acquired from 0–5 km, 5–14.5 km,
213   and 14.5–18.9 km measurements for all flights. Individual data points (5-s averages) are shown by the dots
214   and the averages (by θ of 2K) are shown by the solid squares.
215

3.3 Mechanisms for aerosol enhancement in the TTL

217   We find that the aerosol MMR was tightly correlated with O_3 in the TTL during all flights with
218   small variation between flights. This can be clearly seen in the example time series of O3 and
219   aerosol MMR for the flight on October 18 shown in Fig. 3a. The Pearson's correlation coefficient
220   (r) for the campaign-average O_3 and aerosol MMR (averaged into 2-K θ intervals) was 0.98 in
221   layer III. In contrast, the aerosol MMR and O_3 were anticorrelated with an r value of -0.35 in layer
222   I (Fig. 3b), and no correlation was observed between aerosol MMR and O_3 in layer II.
223
224   The main processes contributing to the increase in TTL O_3 from the bottom to the top of the TTL
225   include chemical production via photolytic dissociation of molecular oxygen (O_2) (Prather 2009;
226   Crutzen et al., 1999) and isentropic in-mixing of stratospheric air from the extratropical lower
227   stratosphere (Konopka et al., 2010; Ploeger et al., 2012). The relative contribution of these
228   processes to O_3 remains unclear. While some studies argue that in situ chemical production
229   dominates (Avallone and Prather 1996), others suggest that isentropic stratospheric in-mixing can
230   contribute to O_3 by as much as 40-60% (Abalos et al., 2013a, 2013b; Konopka et al., 2009, 2010;
231   Ploeger et al., 2011, 2012; Sargent et al., 2014). This contribution is most significant during the
232   boreal summer months (June–August), primarily driven by the Asian summer monsoon, and

233 gradually decreases during transition into the fall and winter months. In particular, these studies
234 suggest that the contribution from in-mixing falls within the range of 0-20% in October, averaged
235 over a ±10°N latitude range, with the contribution increasing with altitude.
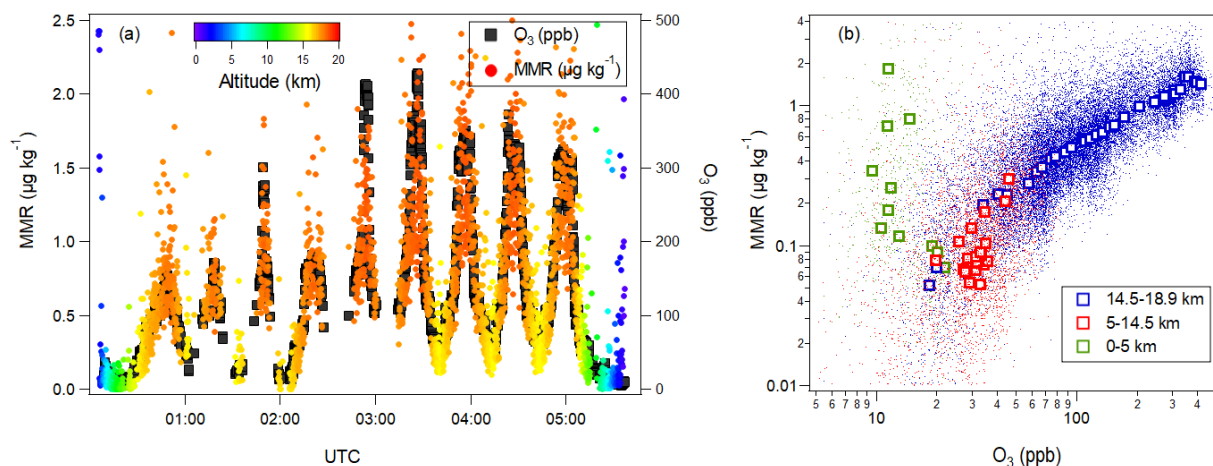236

238 **Figure 3**. **(a)** Example time series of aerosol MMR and O_3 for the October 18 measurements. The gaps
239 indicate ice-influenced data that were excluded from the analysis. **(b)** Scatter plot of MMR vs O_3 for the 0–
240 5 km (layer I), 5–14.5 km (layer II), and 14.5–18.9 km (layer III) measurements. Individual data points are
241 shown by the dots and the averages are shown by the solid squares Logarithmic scales are used to make the
242 small values visible.
243

244 We used a one-dimensional column model (over the flight region) and tracer analysis to examine
245 these processes. The model calculates the vertical distribution of O_3 within the TTL, considering
246 a constant slow vertical ascent rate of 0.25 mm s^{-1} (Park et al., 2010; Avallone and Prather 1996)
247 of air in the TTL and assuming it evolves in isolation (Supporting Information). Remarkably, the
248 calculated vertical profile of O_3 closely aligns with the observed O_3 profile (Fig. 4a). This result is
249 in line with earlier investigations that yielded similar results using a column model (Avallone and
250 Prather 1996) and with research that assumed the tropics are isolated from extra-tropics when
251 explaining the annual cycles of ozone above the tropical tropopause (Randel et al., 2007; Schoeberl
252 et al., 2008). However, we acknowledge the simplicity of the model. For example, the model does
253 not consider the chemistry of nitrogen oxides (NO and NO_2; not measured during POSIDON) and
254 O_3, which could be important in the TTL O_3 abundance (Nussbaumer et al., 2023), and
255 uncertainties exist in the assumed ascent rate. On the other hand, the tracer analysis shows evidence
256 of stratospheric in-mixing. Fig. S4 shows that N_2O was anticorrelated with O_3 in the TTL during
257 POSIDON. The observed negative correlation indicates that the sampled TTL air included a
258 contribution from mixing of stratospheric origin (Folkins et al., 1999). This is because the strong
259 UV radiation at higher altitudes in the stratosphere photolyzes N_2O while leading to O_3 production,
260 resulting in an anticorrelation of N_2O and O_3 (Assonov et al., 2013). In contrast, N_2O in the
261 troposphere is inert and uniformly distributed, thus correlation of N_2O with O_3 is not expected and
262 not observed below the TTL during our measurements. The synthesis of modeling and tracer
263 analysis indicates contributions from both chemical production and stratospheric in-mixing to TTL

264   O_3. Given the strong correlation between O_3 and aerosols in the TTL, these results suggest that
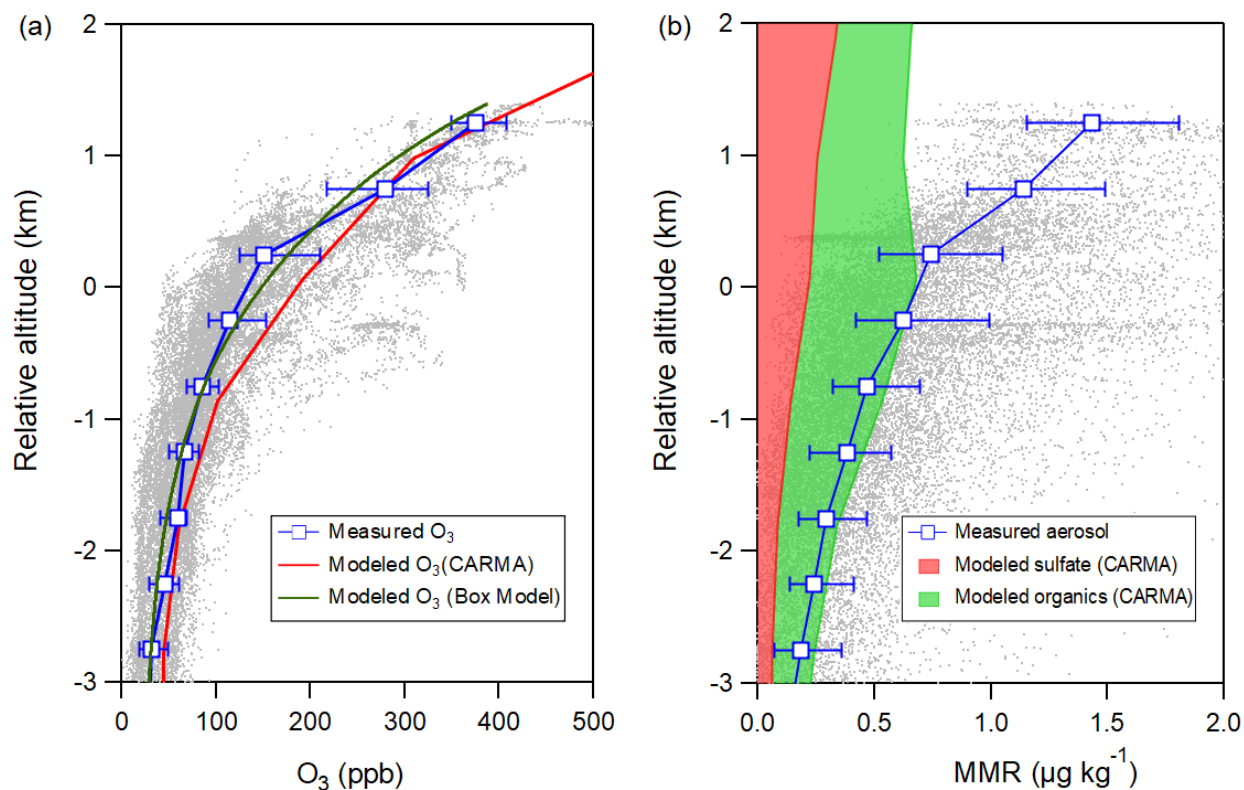265   TTL aerosols may also come from a combination of these chemical and physical processes.
266

267
268   **Figure 4**. Comparison of modeling results to measurements for **(a)** O_3 and **(b)** aerosol MMR. Individual
269   measurement points are shown by the grey dots. The median values and the 25th and 75th percentiles are
270   shown by the blue line-square symbols and the error bars. The y-axis represents altitude relative to the
271   tropopause.
272

273   To investigate the chemical composition of TTL aerosol, we employed the CARMA model
274   embedded in CESM to simulate the aerosol formation and growth processes. The model
275   reproduced the O_3 profile reasonably well (Fig. 4a). Our model results suggest that sulfate aerosol
276   exhibits a consistent increase with altitude, whereas organic aerosol displays an ascending trend
277   below the tropopause but declines above it. Moreover, our modeled vertical profile of the total
278   aerosol MMR demonstrates good agreement with the in situ measurements (Fig. 4b) below the
279   tropopause, with organic aerosol constituting the significant fraction of the aerosol mass. These
280   modeling results imply that sulfur alone is insufficient to explain the observed aerosol mass, and
281   organic precursors may play a pivotal role in the formation and/or growth of TTL aerosols under
282   low-temperature conditions. This finding aligns with previous findings from TTL measurements
283   during the Pre-AVE and CR-AVE campaigns over Southwest Central America in boreal winter
284   (Froyd et al., 2009), which highlighted the prevalence of organic-sulfate particles as the most
285   abundant particle type in the TTL and lower stratosphere. We note that the model underestimates
286   the aerosol mass above the tropopause, with the difference increasing with altitude within the TTL,

287 reaching 60% at an altitude of 1 km above the CPT. Additional research is needed to understand
288 this discrepancy.
289
290 We postulate that TTL aerosols are likely generated through the processes of new particle
291 formation and subsequent growth following convective outflow in the upper troposphere
292 (Williamson et al., 2019). The observed aerosol number size distribution in the TTL suggests
293 particle growth with increasing altitude (Fig. S5), although obtaining measurements of smaller
294 particles would enhance our understanding. During convective transport, soluble species are
295 effectively removed, whereas the insoluble and weakly soluble species can endure washout and
296 gradually ascend upward, with minimal loss, to reach the stratosphere (Bechara et al., 2010). The
297 TTL, characterized by low temperature, low particle surface area density, and high relative
298 humidity, provides ideal conditions for new particle formation and growth. Multiple studies have
299 proposed the upper troposphere as the primary nucleation region (Brock et al., 1995; Weigel et al.,
300 2011), and investigations have revealed the involvement of organics in new particle formation and
301 initial growth in the remote tropical upper troposphere (Kupc et al., 2020). Future measurements
302 analyzing the composition of oxidized organic species will enhance our understanding of particle
303 formation and growth pathways. Exceptional overshooting that crosses the tropical tropopause
304 could also affect the aerosol abundance in the TTL (Vernier et al., 2011). This possibility is
305 examined using H_2O as a tracer. The θ-H_2O profile displayed no spikes above the tropopause (Fig.
306 S6), suggesting the absence of overshooting during the measurements.
307
308 The prevalence of secondary aerosol formation as the primary factor influencing TTL aerosol
309 abundance is in line with the strong correlation between TTL aerosol mass and O_3 in our
310 measurements. Building upon this observation and the underlying mechanisms, we further derived
311 an empirical parameterization of aerosol MMR as a function of O_3 in the TTL using linear
312 regression. The derived relationship is expressed as MMR ($\mu g\,kg^{-1}$) = 0.0074($\pm2.2\times10^{-4}$) × O_3 (ppb)
313 + 0.23 (±0.049), accounting for the 50% mass that was not measured by the POPS instrument.
314 This parameterization could be used to estimate TTL aerosol abundance and for validation of
315 modeled results.
316
317 **4 Conclusions**
318
319 Our aircraft measurements conducted over the western Pacific revealed a vertically stratified
320 aerosol distribution comprised of three distinct layers. The lower-troposphere layer, ranging from
321 0 to 5 km in altitude, exhibited a decrease in aerosol mass with height, primarily influenced by
322 surface-level emissions. The layer between 5 and 14.5 km displayed consistently low aerosol
323 concentrations with minimal variability, indicating effective aerosol removal through deep
324 convection processes. In the TTL, we observed an enhanced aerosol mass that exhibited a strong
325 correlation with O_3. The modeling and tracer analysis suggest that TTL O_3 and aerosols likely
326 originate from a combination of chemical production and stratospheric in-mixing processes.
327 Furthermore, based on the linear relationship observed between aerosol MMR and O_3 in the TTL,
328 we derived an empirical parameterization that allows for the estimation of aerosol MMR as a

329 function of O_3. This parameterization holds potential for validating the simulated TTL aerosol
330 abundance in global models, enabling the simulation of the climate impacts of TTL aerosols.
331

332 Our study also highlights the challenge of accurately predicting aerosol mass, particularly above
333 the tropopause, even for the most advanced models. This underscores the existence of significant
334 gaps in our understanding of the origin and formation mechanisms of aerosols in the TTL. To
335 achieve a more comprehensive understanding of TTL aerosol, it is crucial to conduct future
336 measurements that encompass detailed aerosol chemical composition and gas-phase precursors
337 across different locations and seasons. These endeavors will help diagnose potential deficiencies
338 in the models and validate the modeling results. Consequently, they will lead to an improved
339 comprehension of TTL aerosols and facilitate a predictive understanding of their effects on
340 stratospheric chemistry, clouds, and climate.
341

347 **Data Availability Statement**
348 The aircraft measurements during the POSIDON field campaign are available through the NASA
349 ESPO Data Archive: https://espoarchive.nasa.gov/archive/browse/posidon/WB57
350

351 **References**
352 Abalos, M., Randel, W.J., Kinnison, D.E., & Serrano, E. (2013). Quantifying tracer transport in
353 the tropical lower stratosphere using WACCM. *Atmos. Chem. Phys.*, 13, 10591–10607.
354

355 Abalos et al., Ploeger, F., Konopka, P., Randel, W. J., & Serrano, E. (2013). Ozone seasonality
356 above the tropical tropopause: reconciling the Eulerian and Lagrangian perspectives of transport
357 processes, *Atmos. Chem. Phys.*, 13, 10787–10794.
358

359 Andreae, M. O., Afchine, A., Albrecht, R., Holanda, B. A., Artaxo, P., Barbosa, H. M. J., et al.
360 (2018). Aerosol characteristics and particle production in the upper troposphere over the Amazon
361 Basin. *Atmo. Meas. Tech.*, 18, 921–961.
362

363 Assonov, S. S., Brenninkmeijer, C. A. M., Schuck, T. & Umezawa, T. (2013). N_2O as a tracer of
364 mixing stratospheric and tropospheric air based on CARIBIC data with applications for CO_2.
365 *Atmos. Environ.*, 79, 769–779.
366

367 Avallone, L. M., & Prather, M., J. (1996). Photochemical evolution of ozone in the lower tropical
367 stratosphere. *J. Geophys. Res.*, 101. https://doi.org/10.1029/95JD03010.
368

369 Bechara, J., Borbon, A., Jambert, C., Colomb, A., & Perros, P. E. (2010). Evidence of the impact
370 of deep convection on reactive volatile organic compounds in the upper tropical troposphere during
371 the AMMA experiment in West Africa. *Atmos. Chem. Phys.*, 10, 10321–10334.
372

Brock, C. A., Hamill, P., Wilson, J. C., Jonsson, H. H., & Chan, K. R. (1995). Particle formation in the upper tropical troposphere : A Source of Nuclei for the Stratospheric Aerosol. *Science*, 270, 1650–1653.

Chan, K. R., Scott, S. G., & Bui, T. P. (1989). Temperature and horizontal wind measurements on the ER-2 aircraft during the 1987 airborne Antarctic ozone experiment. *J. Geophys. Res.*, 94, 11573–11587. https://doi.org/10.1029/JD094iD09p11573.

Cui, Y. Y., Liu, S., Bai, Z., Bian, J., Li, D., Fan, K. et al. (2018). Religious burning as a potential major source of atmospheric fine aerosols in summertime Lhasa on the Tibetan Plateau. *Atmos. Environ.*, 181, 186–191.

Crutzen, P. J., Lawrence, M. G., & Poschl, U. (1999). On the background photochemistry of tropospheric ozone. *Tellus*, 51A-B, 123–146.

Folkins, I. & Martin, R. V. (2005). The vertical structure of tropical convection and its impact on the budgets of water vapor and ozone. *J. Atmos. Sci.*, 62(5), 1560–1573.

Folkins, I., Loewenstein, M., Podolske, J., & Oltmans, J. (1999). A barrier to vertical mixing at 14 km in the tropics: Evidence from ozonesondes and aircraft measurements. *J. Geophys. Res.*, 104, 22095–22102. https://doi.org/10.1029/1999JD900404.

Folkins, I., Braun, C., Thompson, A. M., & Witte, J. (2002). Tropical ozone as an indicator of deep convection. *J. Geophys. Res. Atmos.*, 107(13), 1–10. https://doi.org/10.1029/2001JD001178.

Froyd, K. D., Murphy, D. M., Sanford, T. J., Thomson, D. S., Wilson, J. C., Pfister, L., & Lait, L. (2009). Aerosol composition of the tropical upper troposphere. *Atmos. Chem. Phys.*, 9, 4363–4385.

Fueglistaler, S., M. Bonazzola, P. H. Haynes, & Peter T. (2005). Stratospheric water vapor predicted from the Lagrangian temperature history of air entering the stratosphere in the tropics. *J. Geophys. Res.*, 110, D08107, doi:10.1029/2004JD005516.

Fueglistaler, S., Dessler, A. E., Dunkerton, T. J., Folkins, I., Fu, Q., & Mote, P. W. (2009). Tropical tropopause layer. *Rev. Geophys.*, 47, https://doi.org/10.1029/2008RG000267.

Gao, R. S., Ballard, J., Watts, L. A., Thornberry, T. D., Ciciora, S. J., McLaughlin, R. J., & Fahey, D. W. (2012). A compact, fast UV photometer for measurement of ozone from research aircraft, *Atmos. Meas. Tech.*, 5(9), 2201–2210. https://doi.org/10.5194/amt-5-2201-2012.

Gao, R. S., Telg, H., McLaughlin, R. J., Ciciora, S. J., Watts, L. A., Richardson, M. S. et al. (2016). A light-weight, high-sensitivity particle spectrometer for $PM_{2.5}$ aerosol measurements. *Aerosol Sci. Technol.*, 50, 88–99..

Gettelman, A. & Forster, P. M. d. F. (2002). A climatology of the tropical tropopause layer. *J. Meteorol. Soc. Japan*, 80(4B), 911–924. https://doi.org/10.2151/jmsj.80.911.

Hong, Y., Liu, G., & Li, J.-L. F. (2016). Assessing the radiative effects of global ice clouds based on CloudSat and CALIPSO measurements. *J. Climate*, 7651–7674, https://doi.org/10.1175/JCLI-D-15-0799.1.

Jensen, E. J., Diskin, G., Lawson, R. P., Lance, S., Bui, T. P., Hlavka, D. et al. (2013). Ice nucleation and dehydration in the tropical tropopause layer. *Proc. Natl. Acad. Sci.*, 110(6). https://doi/org/10.1073/pnas.1217104110.

Jonsson, H. H., Wilson, J. C., Brock, C. A., Knollenberg, R. G., Newton, R., Dye, J. E. et al. (1995). Performance of a focused cavity aerosol spectrometer for measurements in the stratosphere of particle size in the 0.06-2.0-µm-dimaeter range. *J. Atmos. Ocean. Technol.*, 12, 115–129.

Konopka, P., Grooß, J.-U., Ploeger, F., & Müller, R. (2009). Annual cycleof horizontal in-mixing into the lower tropical stratosphere. *J. Geophys. Res.*, 114, D19111. https://doi.org/10.1029/2009JD011955.

Konopka, P., Grooß, J.-U., Günther, G., Ploeger, F., Pommrich, R., Müller, R., & Livesey, N. (2010). Annual cycle of ozone at and above thetropical tropopause: Observations versus simulations with the ChemicalLagrangian Model of the Stratosphere (CLaMS). *Atmos. Chem. Phys.*,10, 121–132.

Krejci, R., Stro, J., Reus, M. De, Hoor, P., Williams, J. & Fischer, H. (2003). Evolution of aerosol properties over the rain forest in Surinam , South America , observed from aircraft during the LBA-CLAIRE 98 experiment. *J. Geophys. Res.-Atmos*, 108, 1–17. doi:10.1029/2001JD001375.

Kupc, A., Williamson, C. J., Hodshire, A. L., Kazil, J., Ray, E., Bui, T. P. et al. (2020). The potential role of organics in new particle formation and initial growth in the remote tropical upper troposphere. *Atmos. Chem. Phys.*, 20, 15037–15060.

Lance, S., Brock, C. A., Rogers, D., Gordon, J. A., & Oceanic, N. (2010). Water droplet calibration of the Cloud Droplet Probe (CDP) and in-flight performance in liquid , ice and mixed-phase clouds during ARCPAC. *Atmo. Meas. Tech.*, 3, 1683–1706. https://doi:10.5194/amt-3-1683-2010.

Mcfarquhar, G. M., Um, J., Freer, M., Baumgardner, D., Kok, G. L., & Mace, G. (2007). Importance of small ice crystals to cirrus properties: Observations from the Tropical Warm Pool International Cloud Experiment. *Geophys. Res. Lett.*, 34, 1–6. https://doi.org/10.1029/2007GL029865.

Liu, S., Liu, C. C., Froyd K. D., Schill, G. P., Murphy, D. M., Bui, T. P. et al. (2021). Sea spray aerosol concentration modulated by sea surface temperature. *Proc. Natl. Acad. Sci.*, 118(9), https://doi.org/10.1073/pnas. 2020583118.

Mclinden, C. A., McConnell, J. C., McElroy, C. T., & Griffioen, E. (1999). Observations of stratospheric aerosol using CPFM polarized limb radiances. *J. Atmos. Sci.*, 56, 233–240.

Murphy, D. M., Cziczo, D. J., Hudson, P. K., Thomson, D. S., Wilson, J. C., Buseck, P. R. et al. (2004). Particle generation and resuspension in aircraft inlets when flying in clouds particle

generation and resuspension in aircraft inlets when flying in clouds. *Aerosol Sci. Technol.*, 38, 401–409. https://doi.org/10.1080/02786820490443094.

Nussbaumer, C. M., Fischer, H., Lelieveld, J., & Pozzer, A. (2003). What controls ozone sensitivity in the upper tropical troposphere? *Atmos. Chem. Phys.*, 23, 12651–12669.

Penner, J. E., Chen, Y., Wang, M., & Liu, X. (2009). Possible influence of anthropogenic aerosols on cirrus clouds and anthropogenic forcing. *Atmos. Chem. Phys.*, 9(3), 879–896. https://doi.org/10.5194/acp-9-879-2009.

Ploeger, F., fueglistaler, S., Grooß, J.-U., Günther, G., Konopka, P., Liu, Y. S., et al. (2011). Insight from ozone and water vapour on transportin the tropical tropopause layer (TTL). *Atmos. Chem. Phys,* 11, 407–419.

Ploeger, F., Konopka, P., Müller, R., Fueglistaler, S., Schmidt, T., Manners, J. C. et al. (2012). Horizontal transport affecting trace gas seasonality in the Tropical Tropopause Layer (TTL). *J. Geophys. Res.*, 117, D09303. https://doi.org/10.1029/2011JD017267.

Prather, M. J. (2009). Tropospheric O_3 from photolysis of O_2. *Geophys. Res. Lett.*, 36. https://doi:10.1029/2008GL036851.

Randel, W. J. & Jensen, E. J. (2013). Physical processes in the tropical tropopause layer and their roles in a changing climate. *Nat. Geosci.*, 6, 169–176. https://doi/org10.1038/ngeo1733.

Randel, W. J., Park, M., & Wu, F. (2007). A large annual cycle in ozone above the tropical tropopause linked to the Brewer-Dobson circulation. *J. Atmos. Sci.*, 4479–4488.

de Reus, M., Krejci, R., Williams, J., Fischer, H., Scheele, R. & Strom, J. (2001). Vertical and horizontal distributions of the aerosol number concentration and size distribution over the northern Indian Ocean. *J. Geophys. Res.-Atmos*, 106, 629–641. https://doi.org/10.1029/2001JD900017.

Gelaro, R., McCarty, W., Suarez, M. J., Todling, R., Molod, A., Takacs, L. et al. (2017). The Modern-Era Retrospective Analysis for Research and Applications, Version 2 (MERRA-2). *J. Climate*, 5419–5454.

Rollins, A. W., Thornberry, T. D., Watts, L. A., Yu, P., Rosenlof, K. H., Mills, M. et al. (2017). The role of sulfur dioxide in stratospheric aerosol formation evaluated by using in situ measurements in the tropical lower stratosphere. *Geophys. Res. Lett.*, 4280–4286. https://doi.org/10.1002/2017GL072754.

Sargent, M. R., Smith, J. B., Sayres, D. S., & Anderson, J. G. (2014). The roles of deep convection and extratropical mixing in the tropical tropopause layer: An in situ measurement perspective. *J. Geophys. Res.-Atmos*, 12355–12371. https://doi.org/10.1002/2014JD022157.

Schoeberl, M. R., Douglass, A. R., Newman, P. A., Lait, L. R., Lary, D., Waters, J. (2008). QBO and annual cycle variations in tropical lower stratosphere trace gases from HALOE and Aura MLS observations. *J. Geophys. Res.*, 113, D05301. https://doi.org/10.1029/2007JD008678.

Schwarz, J. P., Gao, R. S., Fahey, D. W., Thomson, D. S., Watts, L. A., Wilson, J. C. (2006). Single-particle measurements of midlatitude black carbon and light-scattering aerosols from the boundary layer to the lower stratosphere. *J. Geophys. Res.*, 111. https://doi.org/10.1029/2006JD007076, doi:10.1029/2006JD007076.

Scott, S. G., Bui, P. T. & Chan, R. K. (1990). The meteorological measurement system on the NASA ER-2 aircraft. *J. Atmos. Ocean. Technol.*, 7, 525–540.

Stratosphere-troposphere Processes and their Role in Climate (SPARC), Assessment of Stratospheric Aerosol Properties (ASAP), WCRP-124, WMO/TD No. 1295, SPARC Rep. 4, 2006.

Sunilkumar, S. V., Muhsin, M., Venkat Ratnam, M., Parameswaran, K., Krishna Murthy, B. V., & Emmanuel, M. (2017). Boundaries of tropical tropopause layer (TTL): A new perspective based on thermal and stability profiles. *J. Geophys. Res.*, 741–754, 2017. https://doi.org/10.1002/2016JD025217.

Thornberry, T. D., Rollins, A. W., Gao, R. S., Watts, L. A., Ciciora, S. J., McLaughlin, & Fahey, D. W. (2015). A two-channel, tunable diode laser-based hygrometer for measurement of water vapor and cirrus cloud ice water content in the upper troposphere and lower stratosphere. *Atmos. Meas. Tech.*, 8, 211-224. https://doi.org/10.5194/amt-8-211-2015.

Tolbert, A., Rossi, J. M. & Golden, D. M. (1988). Heterogeneous interactions of chlorine nitrate, hydrogen chloride, and nitric acid with sulfuric acid surfaces at stratospheric temperatures. *Geophys. Res. Lett.*, 15, 847–850. https://doi.org/10.1029/GL015i008p00847.

Toon, O. B., Turco, R. P., Westphal, D., Malone, R., & Liu, M. (1988). A multidimensional model for aerosols—Description of computational analogs. *Journal of the Atmospheric Sciences*, 45(15), 2123–2144.

Vernier, J., Pommereau, J., Thomason, L. W., Pelon, J., Garnier, A., Deshler, T. et al. (2011). Overshooting of clean tropospheric air in the tropical lower stratosphere as seen by the CALIPSO lidar. *Atmos. Chem. Phys.*, 9683–9696. https://doi.org/10.5194/acp-11-9683-2011.

Weigel, R., Borrmann, S., Kazil, J., Minikin, A., Stohl, A., Wilson, J. C. et al. (2011). In situ observations of new particle formation in the tropical upper troposphere: The role of clouds and the nucleation mechanism. *Atmos. Chem. Phys.*, 11, 9983–10010. https://doi.org/10.5194/acp-11-9983-2011.

Weigel, R., Mahnke, C., Baumgartner, M., Dragoneas, A., Vogel, B., Ploeger, F. et al. (2021). In situ observation of new particle formation (NPF) in the tropical tropopause layer of the 2017 Asian monsoon anticyclone – Part 1:Summary of StratoClim results. *Atmos. Chem. Phys.*, 21, 11689–11722.

Williamson, C. J., Kupc, A., Axisa, D., Bilsback, K. R., Bui, T., Campuzano-jost, P. (2019). A large source of cloud condensation nuclei from new particle formation in the tropics. *Nature*, 574,

556   399–403. https://doi.org/10.1038/s41586-019-1638-9.
557
558   Yan, X., Ho, C., Zheng, Q., & Klemas, V. (1992). Temperature and size variabilities of the western
559   pacific warm pool. *Science*, 258, 1643–1645.
560
561   Yu, P., Toon, O. B., Bardeen, C. G., Mills, M. J., Fan, T., English, J. M., & Neely, R. R. (2015).
562   Evaluations of tropospheric aerosol properties simulated by the community Earth system model
563   with a sectional aerosol microphysics scheme. *Journal of Advances in Modeling Earth Systems*,
564   *7*(2), 865–914.
565
566   Yu, P., Rosenlof, K. H., Liu, S., Telg, H., Thornberry, T. D., Rollins, A. W. et al. (2017). Efficient
567   transport of tropospheric aerosol into the stratosphere via the Asian summer monsoon anticyclone.
568   *Proc. Natl. Acad. Sci.*, 114(27), 6972–6977. https://doi.org/10.1073/pnas.1701170114.
569
570   Yu, P., Froyd, K. D., Portmann, R. W., Toon, O. B., Freitas, S. R., Bardeen, C. G. et al. (2019).
571   Efficient in-cloud removal of aerosols by deep convection. Geophysical Research Letters, 46.
572   https://doi.org/10.1029/2018GL080544.
573
574   Zhao, J., & Turco, R. P. (1995). Nucleation simulations in the wake of a jet aircraft in stratospheric
575   flight. *J. Aerosol Sci.*, 26, 779–795.
576
577